Available online at www.sciencedirect.com
ScienceDirect
International Journal of Mass Spectrometry 262 (2007) 211–219
International Journal of Mass Spectrometry
www.elsevier.com/locate/ijms

Trapping and recording the collision- and photo-induced fragmentation patterns of multiply charged metal complexes in the gas phase

Guohua Wu, Daniel Chapman, Anthony J. Stace *

Department of Physical Chemistry, School of Chemistry, The University of Nottingham, University Park, Nottingham NG7 2RD, UK

Received 29 September 2006; received in revised form 15 November 2006; accepted 15 November 2006
Available online 12 December 2006

Abstract

A quadrupole ion trap has been interfaced with a pick-up cluster ion source and a quadrupole mass filter in order to combine the storage capabilities of the trap with the advantages of the pick-up technique for producing a wide variety of multiply charged metal–ligand complexes. Complexes produced using the pick-up technique are ionized by high energy electron impact before passing through a quadrupole mass filter. The mass-selected ions are transmitted by ion guide and injected into a quadrupole ion trap, where they are accumulated for up to 1000 ms and further isolated to remove any reaction/charge transfer fragments. Following collision-induced dissociation (CID) or photoexcitation, ions are ejected from the trap and mass analyzed. CID experiments show that certain dication complexes are very susceptible to the presence of background water in the trap, but that collisional activation can provide a mechanism for revealing stable metal/ligand combinations. The results from preliminary photoexcitation experiments in the form of infrared multi-photon dissociation (IRMPD) are discussed in terms of fragmentation patterns and processes induced by Coulomb explosion. The instrumentation and experimental parameters are presented here together with preliminary results on selected doubly charged complexes containing Cu^{2+}, Mg^{2+} and Zn^{2+}. The apparatus is evaluated in terms of performance with regard to being able to provide sufficient ion signal to store and study the reactivity and spectroscopy of a wide range of multiply charged ions in the gas phase.

Keywords: Metal complexes; Ion trap; Photodissociation; Multiply charged

1. Introduction

Understanding the structure and chemistry of gas phase multiply charged metal/molecule complexes presents considerable experimental challenges [1], many of which arise because of the strong propensity for such complexes to undergo charge reduction. This situation contrast markedly with singly charged complexes where, in the absence of similar problems, considerable progress has been made using such techniques as collision-induced dissociation (CID) [2,3] and photodissociation to investigate the properties of ions [4,5]. For a number of years, infrared multi-photon dissociation (IRMPD) has proven capable of providing a wealth of information on the structures of ions, particularly when complemented with theoretical techniques to calculate vibrational frequencies. For the case of ions held in traps (ICR or quadrupole), the early experiments of Beauchamp and co-workers [6–8] and Eyler and co-workers [9,10] used line tuneable CO_2 lasers to promote IRMPD. The advantage being that stored ions are able to accumulate large numbers of low energy photons, which means that low powered cw lasers, such as the CO_2 laser, can be used. Shin and Beauchamp [8], for example, obtained IRMPD spectra for $Mn(CO)_4CF_3^-$ ion generated from different precursors, and used the spectral similarity provide by a CO_2 laser as evidence of a common structure. More recently, free electron lasers (FEL) have been used in conjunction with ion traps to generate IR spectra covering a much wider wavelength range than is accessible with a CO_2 laser [11,12].

To date, experiments on metal cations have mainly been restricted to singly charged species, which contrasts with the fact that, for a significant fraction of metals in the periodic table, the +2 charge state is more commonly observed as part of their condensed phase chemistry and biochemistry. Since the second ionization energy (IE) of most metal atoms exceeds the first IE of most ligands, charge transfer often prevents the observation of stable multiply charged com-

* Corresponding author.
E-mail address: anthony.stace@nottingham.ac.uk (A.J. Stace).

1387-3806/$ – see front matter © 2006 Elsevier B.V. All rights reserved.
doi:10.1016/j.ijms.2006.11.012

plexes in the gas phase. Many small multiply charged ions are in fact metastable with respect to dissociation into two singly charged ions, and it is this metastability that makes them vulnerable to charge reduction, particularly when they are stored for the purposes of a spectroscopic or kinetic experiment.

Electrospray ionization (ESI), as introduced by Yamashita and Fenn [13], has been shown by Kebarle and co-workers to be capable of producing high yields of solvated, multiply charged ions [14,15]. When used in conjunction with an ion trap, ESI has been very successful in the study of chemical reactivity on the part of a range of metal dications, and when combined with a tuneable laser system, can also be used to produce ions of spectroscopic interest. Electrospray is also the method of choice for producing multiply charged biological molecules. The mechanism of electrospray has been widely discussed [16–20], and although the technique is very versatile in terms of the range of ligands that can be solvated, there are many simple molecules, e.g., NH_3, which cannot be attached to metal dications. However, when used in conjunction with an ion trap, electrospray has been shown to be very effective at generating metal dication complexes for either kinetic or spectroscopic experiments [21,22]. Recent experiments by Walker et al. have also demonstrated the potential of laser vaporization as a mechanism for generating selected doubly charged metal complexes [23].

As an alternative to ESI for the purposes of generating multiply charged metal/ligand complexes, our group has adopted the pick-up technique [24–27], which has been shown to be capable of producing complexes from a wide variety of metals and ligands. Examples of the types of di- and trication complexes that can be generated, range from the very simple, such as $[Cu(Ar)_N]^{2+}$ [26], through to $[Al(CH_3CN)_4]^{3+}$ [28], which has an established solid-state chemistry. In addition, the pick-up technique is capable of generating complexes in charge states that are difficult to assess by other means, for example, those involving silver(II) [29] and gold(II) [30].

To produce multiply charged ions in preparation for chemical and spectroscopic experiments, the pick-up technique has been coupled to a quadrupole mass filter and an ion trap. The work presented here demonstrates that this combination of techniques is capable of producing ions in sufficient number density to trap and promote reactions via either collision-induced dissociation or IRMPD. This paper provides a detailed description of the experimental technique and the parameters within which the apparatus appears to operate effectively. Preliminary results are presented on selected doubly charged complexes containing Cu^{2+}, Mg^{2+} and Zn^{2+}.

2. Apparatus description

The apparatus shown schematically in Fig. 1 has recently been constructed and some aspects of the equipment are still undergoing development. The instrument comprises of five differentially pumped vacuum chambers, covering the following processes: supersonic expansion, beam collimation, metal vaporization and pick-up, quadrupole mass selection and ion trapping.

2.1. Pick-up process and ionization

Argon is passed through a reservoir where solvents are held in the liquid state and where vapor pressure is controlled through either heating or cooling. A mixture of argon and solvent vapor (∼1% of the ligand of interest seeded in 99% argon) undergoes supersonic expansion through a continuous nozzle 50 μm in diameter. The resultant molecule/argon cluster beam is collimated using a 1 mm diameter skimmer before passing through to an oven chamber containing metal vapor produced from a Knudsen effusion cell. Metal atom attachment occurs via a pick-up process that involves the evaporation of rare gas atoms to stabilize neutral metal-containing complexes, and the general approach appears to be applicable to all metals capable of generating sufficient vapor pressure at temperatures below 2000 °C. Notable advantages of this approach over, for example, electrospray are: (i) it can be used to study a range of metal oxidation states in association with molecules that are not readily accessible in the condensed phase, for example CO_2 has proved to be an extremely effective ligand [31]; (ii) the pick-up technique can also be used to prepare complexes in oxidation states that are difficult to achieve in the condensed phase, for example those of gold(II) [30,32]. A disadvantage is that the technique is currently restricted to ligands that are volatile; however, some success has been obtained with a dual pick-up system where involatile ligands are held in a heated reservoir inside the vacuum chamber that houses the nozzle.[1] Previous experimental work has demonstrated that the use of argon as opposed, for example, to helium is crucial to the success of the pick-up technique [33], and separate molecular dynamics simulations have shown that cooling through argon atom evaporation is an integral part of the pick-up mechanism [34].

Experiments have shown [27,31] that the optimum partial pressure of metal required for the production of mixed solvent/metal clusters lies in the range 10^{-1} to 10^{-2} Torr. At higher pressures the cluster beam intensity drops due to scattering, and at lower pressures insufficient numbers of metal atoms are picked up. A shutter at the exit of the effusion cell is used to confirm the identity of clusters containing metal ions. Vacuum is achieved using diffusion pumps for the expansion chamber (8000 l s^{-1}, BOC Edwards) and collimation chamber (2000 l s^{-1}, BOC Edwards). Two turbo pumps (250 l s^{-1}, BOC Edwards) are used on the oven chamber. Experience has shown that adequate pumping at the base and throat of the Knudsen cell is essential if the latter is to function at high temperatures and moderately high background pressures (∼10^{-5} Torr when the cluster beam is transmitted).

The neutral cluster beam then enters a molecular beam ionizer (ABB Extrel), which is positioned approximately 100 cm downstream from the skimmer. Maximum ionization efficiency is

[1] B.J. Duncome, K. Duale, A.J. Stace, unpublished results.

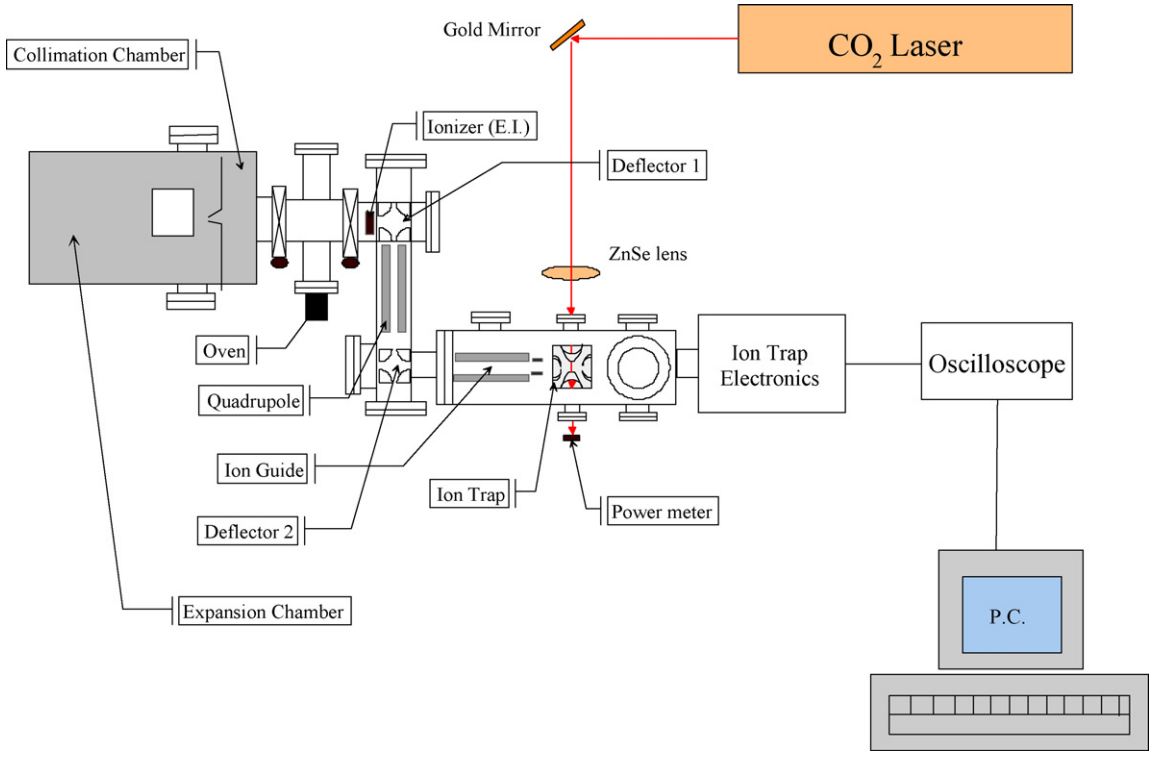

Fig. 1. Schematic diagram of the apparatus, showing the pick-up region (oven), the quadrupole mass filter, and the ion trap, together with ancillary equipment.

achieved using four filament coils connected in a series/parallel combination and mounted on a quadrupole deflector. The latter ensures that unionized material does not contaminate the quadrupole rods. For high ion signals, the filament emission current is set to 5 A and the electron energy to 100 eV. Under these conditions, a quasi-plasma is produced in the ionization region and ion space charge appears to dominate over electron space charge, with the former playing a major role in determining extraction efficiency and final ion signal intensity.

2.2. Ion selection and transmission

Ions with a pre-set kinetic energy are extracted from the ionization region and pass through a quadrupole deflector into a mass filter within which ions of a specific mass to charge ratio are isolated for further study. Mass discrimination on the part of filter is minimized by operating at low resolution. The mass-selected ions are turned through 90° by a second quadrupole deflector before passing through an ion guide and focusing lens and into a three-dimensional radio-frequency quadrupole ion trap (Finngan ITMS system). After accumulation the trapped ions and any reaction products are ejected towards an electron multiplier (Galileo Corporation) located just beyond the exit end cap. At each stage of acceleration and focusing, the energy and dimensions of the ion beam can be optimised for acceptance by tuning the beam through the trap and directly on to the electron multiplier. For this purpose the trap is held at ground potential. Mass spectra and selected ion intensities can also be monitored on a detector located at 180° from the ion guide.

2.3. Ion trapping, storage and isolation

The ion trap is an rf quadrupole trap which operates in the total storage mode, i.e., with zero dc voltage on the two end caps and a 1.1 MHz rf voltage applied to the ring electrode. To trap ions, high purity He (99.9999%) is admitted directly to the ion trap via a precision leak valve (Negretti). Depending on signal intensity, ions are accumulated continuously in the trap for times between 200 and 1000 ms. A set of deflection plates, located immediately before the ion trap are used to 'stop and start' the continuous ion beam, such that ions only enter the ion trap during the 'acquisition' sequence of an experiment. One deflection plate is held at ground potential and the other is pulsed between 0 and 50 V with the latter used to exclude ions from the trap. Ion complexes of interest are preferentially trapped by either dc isolation or by ramping the rf voltage to an appropriate value. This isolation step removes unwanted fragment ions formed by CID or/and ion molecule reactions between injected ions and background molecules; the most reactive being O_2 and water. The latter proved to be a particular problem within the quadrupole and trap chambers and steps taken to minimise the effects of residual water have included cryopumping, baking, and vapor traps on all gas lines.

The quadrupole chamber is pumped by a cryo-cooled diffusion pump (7001 s^{-1}), with a liquid nitrogen cooled baffle fed from a reservoir. The ion trap chamber is pumped by two turbo pumps (2501 s^{-1}, BOC Edwards). The quadrupole and ion trap vacuum chambers are bakeable and are routinely pumped to a background pressure below 3×10^{-8} mbar (uncorrected) after baking at ~100 °C. The pressure is monitored by an ioniza-

tion gauge (Arun Microelectronics Ltd., Gauge controller model PGC2D).

2.4. Photodissociation of trapped ions

Following injection, thermalization, and isolation the mass-selected ions are held in the ion trap for a further 50 ms, during which time they are subjected to infrared excitation from a line-tuneable CO_2 laser. The latter is operated in a chopped cw mode with a pulse duration (20 ms) timed to match the residence time of ions in the trap. The laser beam (<5 mm in diameter) is focused by a ZnSe lens with a focal length of 50 cm and enters the ion trap vacuum chamber via a 50 mm diameter, 4 mm thick ZnSe window mounted on Viton O-rings. The laser beam passes radially through the center of the ion trap with an entrance and exit that are defined by two 1 mm-diameter holes in the ring electrode. Finally the laser beam exits the vacuum chamber via a ZnSe window, where it strikes a power meter (Coherent Model FM, head model LM10). The rf coil of the ITMS system has been re-tuned to compensate for the presence of holes in the ring electrode.

All photodissociation results reported below were recorded with the ion trap operating in a mass-selective instability mode that is initiated 2 ms after the laser pulse. The ion signals were amplified (see below) and recorded on a digital oscilloscope (LeCroy LT374M), which is triggered, together with the CO_2 laser, by TTL signals from a delay/pulse generator (Stanford Research DG535). The delay generator receives a TTL pulse from the scan acquisition PCB on the ITMS system, which in turn is controlled within a single ITMS scan function. ITMS software (Finngan MAT, Revision B) controls the timing sequence of events within the ion trap, such as the rf voltage, through a scan function. A typical scan function and the timing sequence for the pulsed ion deflector and the laser pulse are shown in Fig. 2. All mass spectra shown below represent averages taken of 200 ion trap scan functions (termed microscans within the ITMS software). The data were transferred from the scope to a PC using LeCroy Scope Explorer software via the GPIB port. Typical duty cycles range from 500 to 1200 ms depending primarily on signal intensity, which in turn determines the accumulation time.

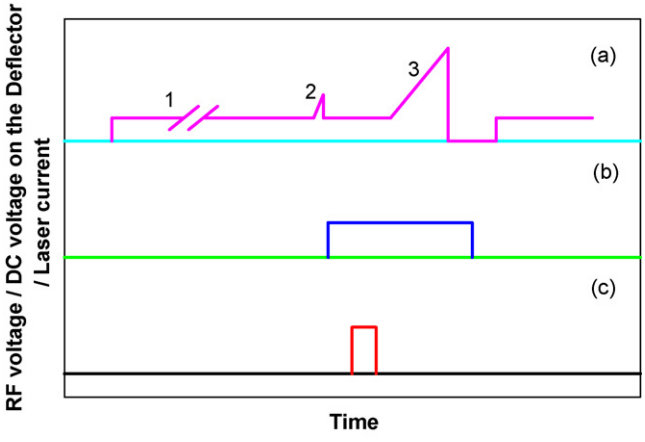

Fig. 2. Timing diagram depicting a typical scan mode for ion injection through to photodissociation. (a) rf voltage levels: (1) ion injection; (2) ion isolation; (3) analytical rf ramp. (b) Deflector voltage (ion gate). (c) Laser irradiation pulse. The duration of the CO_2 laser pulse is 20 ms.

2.5. Preparation of zinc, magnesium, and copper dication complexes with pyridine

Pyridine (Spectrometric grade), zinc (2–14 mesh), and magnesium (granules) were obtained from Aldrich. The copper was from pieces of used gasket. For zinc, the effusion cell operates most effectively when the temperature is held at 380 °C, as measured with a standard C-type thermocouple. The appropriate temperatures for magnesium and copper were 480 and 1370 °C, respectively. Behind the expansion nozzle the argon pressure was held at 140 psi, which gave operating pressures of 4×10^{-5}, 2×10^{-6}, and 5×10^{-7} Torr, respectively, in the expansion, collimation and ion source chambers.

3. Results and discussion

Central to the success of these experiments is the ability of the trap to accumulate sufficient ions to yield quantitative photodissociation signals. Therefore, this section begins with a quantitative analysis of the operating parameters which influence that process within the experiment.

3.1. Total ion current

Experiments showed that a good signal-to-noise ratio could be achieved if individual ion signals on a digital oscilloscope are at least 0.2 V in magnitude. The current from the ion trap is converted to a voltage through a 10 MΩ resistor; therefore, 0.2 V corresponds to an ion signal of 20 nA. The time scale over which the integrator operates is approximately 27 μs, and with a multiplier gain of 10^5, the above current corresponds to 34 ions. However, each ion peak in a recorded ITMS mass spectrum is represented by 15 data points in a distribution that is approximately Gaussian; hence, the total number of the ions ejected from the trap at a given mass should be approximately 230 if the most intense data point corresponds to 15% of the total ion signal. If the trapping efficiency for ions injected from an external source is of the order of 1%, then approximately 23,000 ions in total need to enter the trap. Since the injected ion beam is continuous, the total number of ions reaching the ion trap during the accumulating time should be:

$$N = \frac{I \times t \times 10^{-12}}{1.602 \times 10^{-19} \times G}$$

where I is the ion current in pA, as measured at the second detector with the ring electrode at ground potential, t the accumulation time in s, and G is the multiplier gain. A minimum initial current of approximately 370 pA is required if the accumulation time is 1 s and G is 10^5. Experiments show that this initial condition is not difficult to achieve for many of the metal dication complexes of interest. Moreover, the accumulation time can be modified (within limits) to suit the initial signal strengths of selected ions.

3.2. Buffer gas influence on trapping efficiency and photodissociation

Ion traps are typically operated with moderately high pressures (helium at ~1 mTorr) of buffer gas, the purpose of which is to improve performance (sensitivity and mass resolution) by damping the motion of ions and containing their movement to the center of the trap. Helium is bled directly into the trap and the subsequent gas pressure is monitored on an ion gauge situated some distance from the trap. An accurate measure of helium pressure in the trap was achieved via a calculation of the flow conductance and pumping speeds as follows: the ion trap has seven holes, each 1 mm in diameter in the exit end cap, two holes, each 1 mm in diameter in the ring electrode (entrance and exit for the laser beam), and one 5 mm diameter hole in the entrance end cap. These can be treated as apertures for the purposes of calculating molecular flow conductance using the following equation:

$$C = 3.64\left(\frac{T}{M}\right)^{1/2} A \tag{1}$$

where C is the molecular flow conductance of an aperture in $1\,s^{-1}$, M the molecular mass, T the absolute temperature, and A is the area of an aperture area in cm^2. The total conductance, C, is given by:

$$C = C_1 + C_2 + \cdots + C_n \tag{2}$$

where C_i is the conductance of each aperture. From the definition of conductance

$$C = \frac{Q}{\Delta P} = \frac{Q}{P_1 - P_2} \tag{3}$$

where Q is the total molecular flow, P_1 the upstream pressure, which in this case is the pressure in the ion trap, and P_2 is the downstream pressure, which is the pressure measured on an ion gauge located in a vacuum chamber that contains the trap. The total flow due to the pumps is

$$Q = P_2 \times S \tag{4}$$

where S is the speed of the pumps at the pressure P_2. From Eqs. (3) and (4), P_1 can be calculated as

$$P_1 = \left(1 + \frac{S}{C}\right) \times P_2 \tag{5}$$

C can be calculated using Eqs. (1) and (2) in conjunction with the known speeds of the pumps, and P_2 is recorded on an ion gauge. Hence, the helium pressure in the ion trap can be calculated. Two turbomolecular pumps are used on the ion trap chamber, each with a pumping speed of $250\,l\,s^{-1}$ for helium; however, the inlet screens to the pumps reduce their speed by approximately 10%, and the pumps are also connected to the vacuum system via short sections of tubing. Therefore, the actual pumping speed is given by

$$S_c = \frac{S_n \times C_P}{S_n + C_P} \tag{6}$$

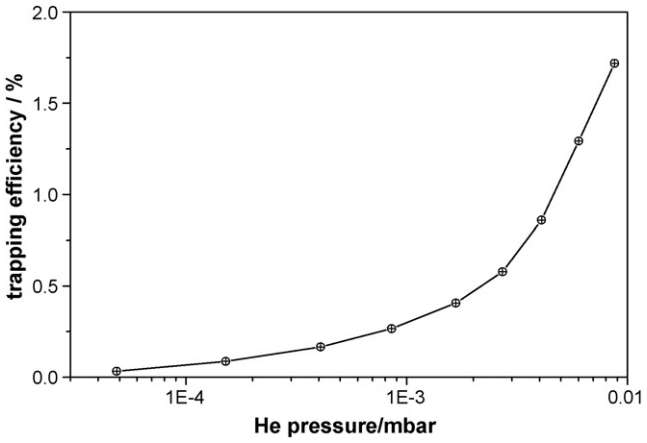

Fig. 3. Effect of helium pressure on the trapping efficiency of dication complexes. Measurements were made on $[^{64}Zn(pyridine)_4]^{2+}$ injected with a laboratory-frame kinetic energy of 22 eV.

where S_n is the nominal pumping speed and C_P is the conductance of the tubing between the pump and the vacuum chamber. The actual pumping speed S_c should be used in place of S in Eq. (5). Finally, it is necessary to correct the ion gauge reading for helium; therefore, the true pressure in the vacuum chamber is given by

$$P_2 = \frac{P_I}{\beta} \tag{7}$$

where P_I is the pressure reading on the ionization gauge, and β is the relative sensitivity of the gauge to helium, which is 0.25. Combining expressions (5), (6) and (7) gives

$$P_1 = \left(1 + \frac{S_n \times C_P}{(S_n + C_P)C}\right) \times \frac{P_I}{\beta} \tag{8}$$

Fig. 3 shows the relation between helium pressure, P_1, and the trapping efficiency of $Zn(pyridine)_4^{2+}$ complexes. The presence of helium focuses ions to the center of the ion trap both radially and axially by quenching their kinetic energy through collisions. The overall shape of the plot matches previous observations by Cooks and co-workers for singly charged ions [35]. As can be seen from Fig. 3, high pressures of helium increase the trapping efficiency; however, with reference to the laser-based experiments, it should be noted that helium is also responsible for collisional deactivation and the quenching of photoexcited ions during the IRMPD process. To separate kinetic energy quenching from photoexcitation, Yost and co-workers [36] incorporated a pulsed helium inlet arrangement into the ion trap scan function. Their results demonstrated improvements in both the trapping efficiency of ions injected from an electrospray source and in the yield of photofragments. Photodissociation experiments performed in the apparatus described above show that collisional deactivation begins to dominate events once the helium pressure is higher than 8.5×10^{-4} mbar (however, the precise value is related to laser power). Therefore, most of the experiments performed here were undertaken at a nominal trap pressure of 1.5×10^{-4} mbar.

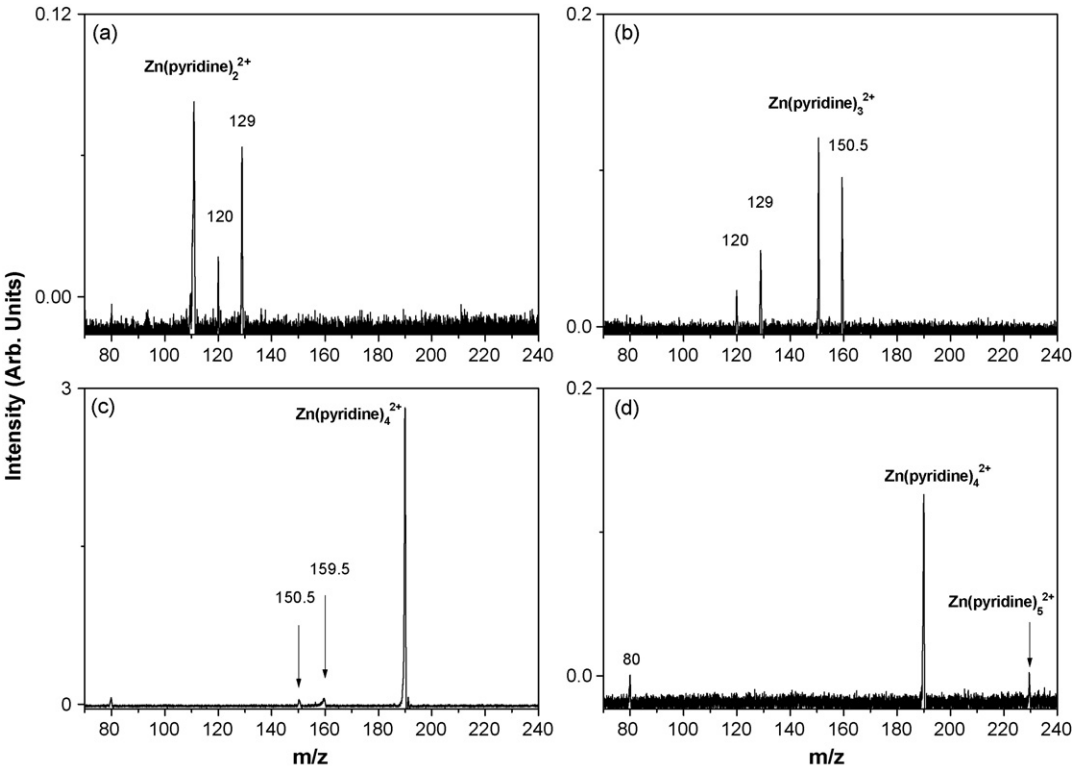

Fig. 4. Ion trap mass spectra recorded following the injection of different $[^{64}Zn(pyridine)_N]^{2+}$ complexes ($N = 2$–5) into the ion trap. (a) $[^{64}Zn(pyridine)_2]^{2+}$, (b) $[^{64}Zn(pyridine)_3]^{2+}$, (c) $[^{64}Zn(pyridine)_4]^{2++}$, and (d) $[^{64}Zn(pyridine_5]^{2+}$.

3.3. The effects of residual water

Fig. 4 shows mass spectra recorded for four doubly charged complex ions $[^{64}Zn(pyridine)_N]^{2+}$ ($N = 2$–5), all of which were injected separately into the trap and stored for 1000 ms. The mass spectrum for $[^{64}Zn(pyridine)_2]^{2+}$ shown in Fig. 4a has additional ions at m/z 120 and 129, which are $[^{64}Zn(H_2O)(pyridine)_2]^{2+}$ and $[^{64}Zn(H_2O)_2(pyridine)_2]^{2+}$, respectively. These products arise from parent ions that have picked up one and two water molecules during their residence time in the trap. The coordination never increases beyond four molecules, but the intensity of $[^{64}Zn(H_2O)_2(pyridine)_2]^{2+}$ continues to rise as a function of trapping time, which suggests that four-coordinate Zn^{2+} may be a stable structure in the gas phase. Similarly, when $[^{64}Zn(pyridine)_3]^{2+}$ is injected into the trap, this ion picks up a single water molecule, as shown in Fig. 4b. However, ions also appear at m/z 120 and 129, which suggests that $[^{64}Zn(H_2O)(pyridine)_2]^{2+}$ and $[^{64}Zn(H_2O)_2(pyridine)_2]^{2+}$ can be formed through the loss of pyridine by either $[^{64}Zn(pyridine)_3]^{2+}$ or $[^{64}Zn(H_2O)(pyridine)_3]^{2+}$ followed by the attachment of a water molecule. These processes would imply that either the Zn^{2+}–pyridine bond in $[^{64}Zn(pyridine)_3]^{2+}$ is weak, or that the three-coordinate ion is vulnerable to attack from a fourth molecule, and that water wins because of abundance (see below).

Fig. 4c shows a mass spectrum recorded for $[^{64}Zn(pyridine)_4]^{2+}$, where the fragments at $m/z = 80$, 150.5 and 159.5 are protonated pyridine ($C_5H_5NH^+$), $[^{64}Zn(pyridine)_3]^{2+}$ and $[^{64}Zn(H_2O)(pyridine)_3]^{2+}$, respectively. As before, these ions are formed by a combination of CID and ion–molecule reactions between injected $Zn(pyridine)_4^{2+}$ ions and background molecules. However, it is clear that the intensities of the product ions are low compared with that of $[^{64}Zn(pyridine)_4]^{2+}$, which means that the latter is probably more stable with respect to both CID and ion–molecule reactions than most of the other dication examples shown in Fig. 4. Finally, Fig. 4d shows a mass spectrum recorded following the injection of $[^{64}Zn(pyridine)_5]^{2+}$ into the ion trap. The most intense peak at m/z 190 is $[^{64}Zn(pyridine)_4]^{2+}$, which arises from the loss of a single pyridine molecule, and the relative intensities of $[^{64}Zn(pyridine)_4]^{2+}$ and $[^{64}Zn(pyridine)_5]^{2+}$ would suggest that the fifth molecule is only weakly bonded to $[^{64}Zn(pyridine)_4]^{2+}$. Taken together with the other mass spectra, the results from Fig. 4d also suggests that reactivity on the part of $[^{64}Zn(pyridine)_N]^{2+}$ complexes proceeds via the direct attack of a vacant site on the zinc cation rather than via ligand exchange. For a closed-shell cation, such as Zn^{2+}, the binding energies of ligands might be expected to decline as a function of increasing N. Therefore, $[^{64}Zn(pyridine)_4]^{2+}$ should be more susceptible than $N = 2$ and 3 to ligand exchange, but will offer greater steric resistance to direct attack by water.

Fig. 5 shows an ion trap mass spectrum recorded when $[^{24}Mg(pyridine)_4]^{2+}$ is injected into the trap. As can be seen, the result is very different from that obtained for $[^{64}Zn(pyridine)_4]^{2+}$. In addition to the parent ion, there is a doubly charged CID fragment, $[^{24}Mg(pyridine)_3]^{2+}$, but these are accompanied by a range of charge transfer fragments, namely:

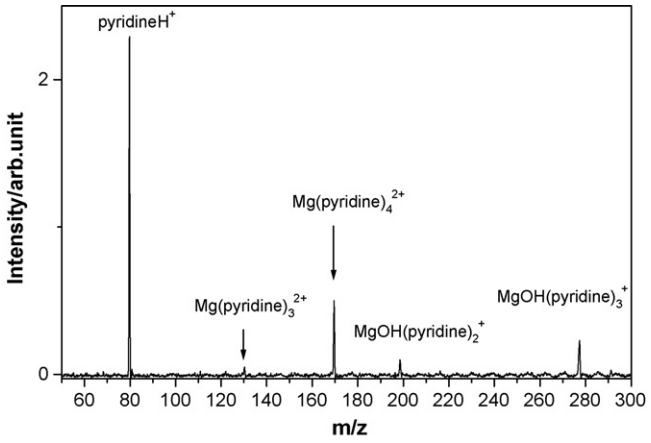

Fig. 5. Ion trap mass spectrum of $[Mg(pyridine)_4]^{2+}$, acquired by examined the contents of the ion trap after $Mg(pyridine)_4^{2+}$ had been injected continuously into the ion trap for 1000 ms.

$MgOH(pyridine)_3^+$, $MgOH(pyridine)_2^+$, and protonated pyridine ($C_5H_5NH^+$). It would appear that $[Mg(pyridine)_4]^{2+}$ is very much more susceptible than $[Zn(pyridine)_4]^{2+}$ to attack by water and that the barrier to hydrolysis for Mg^{2+} is much lower than that of Zn^{2+}. Given the high intensity of $C_5H_5NH^+$, the most probable fragmentation route would appear to be:

$$[Mg(pyridine)_4]^{2+} + H_2O \longrightarrow MgOH(pyridine)_3^+ + pyridineH^+ \quad (9)$$

It is interesting to note that in the bulk phase, Zn^{2+} is seen as a stronger acid (lower pK_h) than Mg^{2+}; however, the course of reaction (9) may be driven by ligand preference, with Zn^{2+} favouring coordination with nitrogen-donating ligands [37], whereas Mg^{2+} preferring oxygen as a donor atom [31].

3.4. IRMPD experiments on $[Zn(pyridine)_{3,4}]^{2+}$ and $[Cu(pyridine)_4]^{2+}$

Fig. 6 shows a shows a short section of a mass spectrum covering the mass range *m/z* 175–230, which was obtained by scanning the quadrupole field following the ionization of an

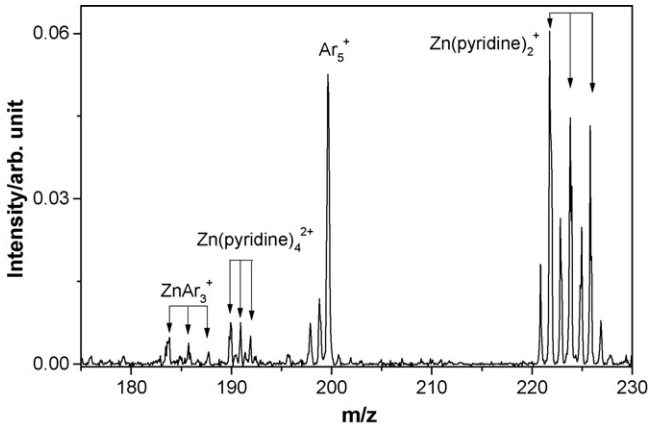

Fig. 6. Short section of a quadrupole mass spectrum recorded over the region where $[Zn(pyridine)_4]^{2+}$ complexes are present. Peaks due to isotopes ^{64}Zn, ^{66}Zn, and ^{68}Zn have been identified.

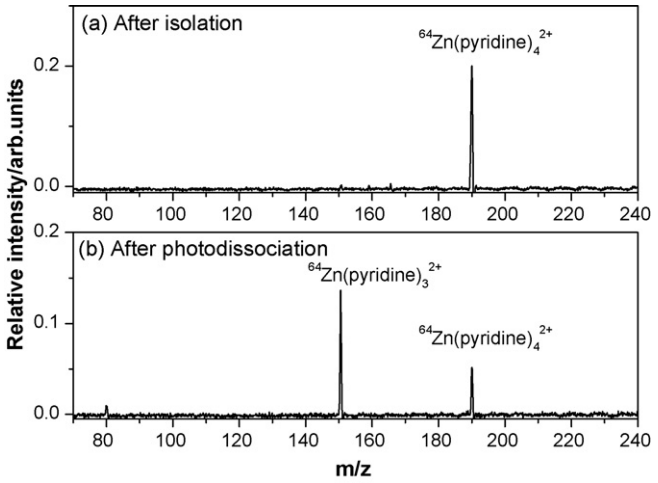

Fig. 7. (a) Ion trap mass spectrum obtained by injecting $[^{64}Zn(pyridine)_4]^{2+}$ into the trap and accumulating for 1000 ms. The quadrupole mass spectrum from which this ion was mass-selected is shown in Fig. 6, and the ion trap mass spectrum prior to the isolation of $[^{64}Zn(pyridine)_4]^{2+}$ is shown in Fig. 4(c). (b) An ion trap mass spectrum recorded following the IRMPD of $[^{64}Zn(pyridine)_4]^{2+}$ through irradiation with IR photons with an energy of 1070.5 cm^{-1}.

expansion where zinc atoms were complexed with mixed pyridine/argon clusters. The mass spectrum consists of ions composed of various combinations of the neutral constituents present in the beam that first enters the ion source. The three peaks at *m/z* 190, 191, and 192 are $[^{64}Zn(pyridine)_4]^{2+}$, $[^{66}Zn(pyridine)_4]^{2+}$, and $[^{68}Zn(pyridine)_4]^{2+}$, respectively. Zinc ions complexed with argon are also produced under these experimental conditions and these are seen at *m/z* 184, 186, 188 and correspond to $^{64}ZnAr_3^+$, $^{66}ZnAr_3^+$, $^{68}ZnAr_3^+$, respectively. Other singly charged ions seen at between *m/z* 221 and 227 are various combinations of protonated, normal and deprotonated complexes derived from $^{64}Zn(pyridine)_2^+$, $^{66}Zn(pyridine)_2^+$, and $^{68}Zn(pyridine)_2^+$. Finally, the intense peak at *m/z* 200 is Ar_5^+.

Fig. 7a shows an ion trap mass spectrum, obtained by mass-selecting and injecting $[^{64}Zn(pyridine)_4]^{2+}$ into the trap, where it has been accumulated for 1000 ms before undergoing a further isolation stage. With only $[^{64}Zn(pyridine)_4]^{2+}$ remaining in the trap the ion was irradiated with 1070.5 cm^{-1} photons from a CO_2 laser at a power of 500 mW. With the laser wavelength in resonance with an allowed infrared transition in the complex, photodissociation occurs via the loss of a single neutral pyridine molecule (Fig. 7b).

$$Zn(pyridine)_4^{2+} + nh\nu \longrightarrow Zn(pyridine)_3^{2+} + pyridine \quad (10)$$

Away from resonance the mass spectrum is essentially the same as that shown in Fig. 7a. An increase in laser power, promotes further dissociation down to $[^{64}Zn(pyridine)_2]^{2+}$.

Fig. 8 shows two further examples of IRMPD within mass-selected ions that have been trapped. Fig. 8a shows the photofragmentation pattern recorded when $[^{64}Zn(pyridine)_3]^{2+}$ is irradiated at 1048.66 cm^{-1} and at the higher laser power of 900 mW. In this example, photoexcitation promotes extensive charge transfer, which is accompanied by the breaking of chemical bonds with pyridine, as opposed to metal–ligand bonds. For a system such as this, a typical response to collision-

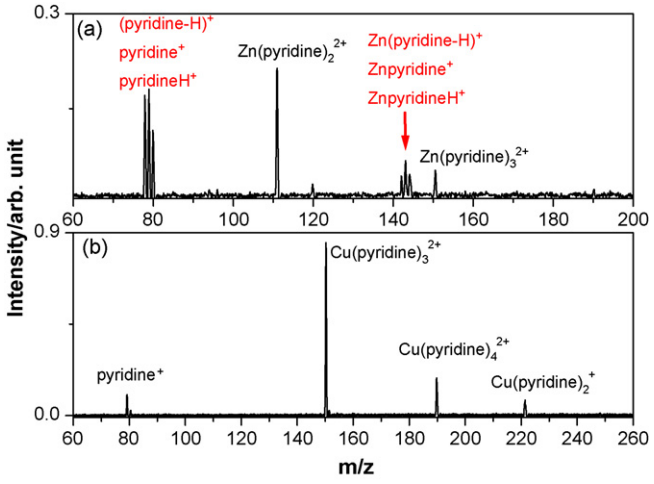

Fig. 8. Ion trap mass spectra obtained following the IRMPD of: (a) $[^{64}Zn(pyridine)_4]^{2+}$ at 1048.66 cm^{-1} with a laser pulse power of 900 mW; (b) $[^{63}Cu(pyridine)_4]^{2+}$ at 1046.86 cm^{-1} with a laser pulse power of 550 mW.

induced charge transfer, would be the formation of protonated pyridine, $C_5H_5NH^+$, and such a product is seen in Fig. 8a. However, the mass spectrum shows two further fragments, one of which corresponds to the addition of a proton to Zn^{2+} leading to the possible formation of the strong Zn^+–H bond. Finally, Fig. 8b shows a mass spectrum recorded following an IRMPD experiment on $[^{63}Cu(pyridine)_4]^{2+}$ at the lower laser power of 550 mW. As can be seen, this also results in charge transfer, but the dominant non-metallic product is $C_5H_5N^+$. Interestingly, there is no complementary $^{63}Cu(pyridine)_3^+$, which suggests that the reaction pathway may be sequential and involve the loss of neutral pyridine from $[^{63}Cu(pyridine)_4]^{2+}$ followed by further photoexcitation to yield $C_5H_5N^+$ and $^{63}Cu(pyridine)_2^+$. IRMPD spectra recorded for selected $[M(pyridine)_4]^{2+}$ complexes have been presented elsewhere [38], and the photon energies quoted above correspond to the peaks of the observed absorption profiles. The vibrational modes responsible for infrared absorption are located on the pyridine molecules.

4. Conclusion

We report here a new apparatus for studying the collision- and photo-induced fragmentation of mass-selected metal dication complexes. These preliminary results demonstrate that the pick-up technique is capable of yielding sufficient ion signal intensity for quantitative experiments on the chemistry of Cu^{2+}, Mg^{2+} and Zn^{2+} complexed with pyridine. The results also show that IRMPD can be applied to systems with high binding energies (here, ~300 kJ/mol), and that with comparatively modest laser powers, photofragmentation can be promoted in dication complexes held within an ion trap.

Several improvements could still be made to further improve the performance of this apparatus. First, the sensitivity can be increased further by improving the base pressure in the quadrupole and ion trap chambers, thus reducing ion–molecule reactions and CID processes between the ions of interest and background molecules, for example, water. Secondly, the implementation of a continuously tuneable light source (FEL or dye laser) will improve the quality of spectra recorded and finally, spectral resolution might be improved by cooling the trapped ions.

Acknowledgement

The authors thank EPSRC for financial support for the construction of this apparatus.

References

[1] A.J. Stace, J. Phys. Chem. 106 (2002) 7993.
[2] J.A. Leary, P.B. Armentrout, Int. J. Mass Spectrom. 204 (2001) ix.
[3] M.T. Rodgers, P.R. Armentrout, Mass Spectrom. Rev. 19 (2000) 215.
[4] R.C. Dunbar, Int. J. Mass Spectrom. 200 (2000) 571.
[5] M.A. Duncan, Int. J. Mass Spectrom. 200 (2000) 545.
[6] C.A. Wight, J.L. Beauchamp, J. Am. Chem. Soc. 103 (1981) 6499.
[7] L. Thorne, J.L. Beauchamp, Gas Phase Ion Chemistry, vol. 3, Academic, Orlando, 1984.
[8] S.K. Shin, J.L. Beauchamp, J. Am. Chem. Soc. 112 (1990) 2057.
[9] D.M. Peiris, M.A. Cheeseman, R. Ramanathan, J.R. Eyler, J. Phys. Chem. 97 (1993) 7839.
[10] D.M. Peiris, J.M. Riveros, J.R. Eyler, Int. J. Mass Spectrom. Ion Processes 159 (1996) 169.
[11] J. Oomens, A.J.A. van Roij, G. Meijer, G. von Helden, Astrophys. J. 542 (2000) 404.
[12] D. van Heijnsbergen, G. von Helden, G. Meijer, P. Maitre, M.A. Duncan, J. Am. Chem. Soc. 124 (2002) 1562.
[13] M. Yamashita, J.B. Fenn, J. Phys. Chem. 88 (1984) 4451.
[14] A.T. Blades, P. Jayaweera, M.G. Ikonomou, P. Kebarle, J. Chem. Phys. 92 (1990) 5900.
[15] A.T. Blades, P. Jayaweera, M.G. Ikonomou, P. Kebarle, Int. J. Mass Spectrom. Ion Processes 102 (1990) 251.
[16] J.V. Iribarne, B.A. Thomson, J. Chem. Phys. 64 (1976) 2287.
[17] P. Kebarle, L. Tang, Anal. Chem. 65 (1993) 972A.
[18] P. Kebarle, Y Ho, in: R.B. Cole (Ed.), Electrospray Ionization Mass Spectrometry: Fundamentals, Instrumentation and Applications, Wiley, New York, 1997, p. 3.
[19] J.N. Smith, R.C. Flagan, J.L. Beauchamp, J. Phys. Chem. A 106 (2002) 9957.
[20] J.B. Fenn, Int. J. Mass Spectrom. 200 (2000) 459.
[21] C.J. Thompson, J. Husband, F. Aquirre, R.B. Metz, J. Phys. Chem. A 104 (2000) 8155.
[22] M.Y. Combariza, R.W. Vachet, J. Phys. Chem. A 108 (2004) 1757.
[23] N.R. Walker, G.A. Grieves, J.B. Jaeger, R.S. Walters, M.A. Duncan, Int. J. Mass Spectrom. 228 (2003) 285.
[24] C.A. Woodward, M.P. Dobson, A.J. Stace, J. Phys. Chem. A 101 (1997) 2279.
[25] A.J. Stace, N.R. Walker, S. Firth, J. Am. Chem. Soc. 119 (1997) 10239.
[26] N.R. Walker, R.R. Wright, P.E. Barran, H. Cox, A.J. Stace, J. Chem. Phys. 114 (2001) 5562.
[27] R.R. Wright, N.R. Walker, S. Firth, A.J. Stace, J. Phys. Chem. A 105 (2001) 54.
[28] L. Puškar, K. Tomlins, B.J. Duncombe, H. Cox, A.J. Stace, J. Am. Chem. Soc. 127 (2005) 7559.
[29] N.R. Walker, R.R. Wright, A.J. Stace, J. Am. Chem. Soc. 121 (1999) 4837.
[30] N.R. Walker, R.R. Wright, P.E. Barran, A.J. Stace, Organometallics 18 (1999) 3569.
[31] N.R. Walker, M. Dobson, R.R. Wright, P.E. Barran, J.N. Murrell, A.J. Stace, J. Am. Chem. Soc. 122 (2000) 7751.

[32] N.R. Walker, R.R. Wright, P.E. Barran, J.N. Murrell, A.J. Stace, J. Am. Chem. Soc. 123 (2001) 4223.
[33] J.F. Winkel, A.B. Jones, C.A. Woodward, D.A. Kirkwood, A.J. Stace, J. Chem. Phys. 101 (1994) 9436.
[34] G. Del Mistro, A.J. Stace, Chem. Phys. Lett. 196 (1992) 67.
[35] J.N. Louris, J.W. Amy, T.Y. Ridley, R.G. Cooks, Int. J. Mass Spectrom. 88 (1989) 97.
[36] S.M. Boue, J.L. Stephenson, R.A. Yost, Rapid Commun. Mass Spectrom. 14 (2000) 1391.
[37] B.J. Duncombe, L. Puškar, B. Wu, A.J. Stace, Can. J. Chem. 83 (2005) 1994.
[38] G. Wu, J. Guan, G.D.C. Aitken, H. Cox, A.J. Stace, J. Chem. Phys. 124 (2006) 201103.